VOL. 19, NO. 6, MARCH 2024 ISSN 1819-6608
ARPN Journal of Engineering and Applied Sciences

www.arpnjournals.com

NUMERICAL STUDY OF AERODYNAMICS DRAG AND FLOW CHARACTERISTICS OF THE HIGH-SPEED TRAIN HEAD DESIGN

Beny Halfina, Muhammad Muhammad, Andik Dwi Kurniawan, Khoerul Anwar, Guino Verma, Jean Mario Valentino, Irfan Ansori and Barep Luhur Widodo
Research Center for Transportation Technology, National Research and Innovation Agency, Kawasan Sains dan Teknologi (KST) BJ Habibie, Serpong, South Tangerang, Indonesia
E-Mail: beny002@brin.go.id

ABSTRACT

A native design of the Indonesian high-speed train has been developed as an improvement of the previous medium-speed train model. As the design speed is proposed to be increased from 160 km/h to 250 km/h, the nose shape and nose length of the train head were modified into a sharper and longer nose. In this study, numerical simulation of computational fluid dynamics was used to investigate the aerodynamic phenomena and flow behavior around the modified train head and carbodies. The CFD simulation was used as the verification of the shape design and a tool for rapid design changes and optimization. The model configuration is three cars on a real scale by ignoring other parts like the train window and door, pantograph, and train connecting. A k-ε turbulence model was used in the simulation. From this investigation, it is found that the coefficient of drag on the model is calculated to be 0.34. Meanwhile, an experimental wind tunnel test validates the result with a coefficient drag is 0.38 or 10% divergence from the numerical method.

Keywords: high-speed train (HST); aerodynamic drag; numerical simulation; train aerodynamics; drag coefficient.

Manuscript Received 22 January 2024; Revised 16 March 2024; Published 15 May 2024

1. INTRODUCTION

The high-speed train (HST) aerodynamics study has been an intriguing research issue. During train operation, the drag force increases rapidly and becomes the dominant component of the overall resistance force. Despite extensive studies towards reducing aerodynamic drag, the development of a local design for the Indonesian HST is new and limited. Design iteration is required to construct the optimum design.

Because of the high expense of producing the model and conducting practical tests in a wind tunnel, numerical analysis is the most cost-effective approach for validating the design under development. The numerical study of a high-speed train refers to the implementation of computational tools to model and analyze the airflow behavior of an HST as it moves through the air. The airflow structure around the train will be significantly influenced by the train head, in terms of nose shape and nose length [1]. The train head's aerodynamic properties substantially impact on entire performance, including speed, energy consumption, and stability. Moreover, engineers can also improve aerodynamic performance, reduce drag, reduce noise, and boost speed by employing computational methods to simulate and optimize the train head shape and design. As a result, train aerodynamics, particularly on the train head, is both interesting and challenging.

Much research has been conducted to investigate the many aspects that influence aerodynamic properties. The slenderness ratio of an HST head affects the aerodynamic characteristics of the trainset. When the slenderness ratio is small, the pressure drag will be dominant on the whole aerodynamic train, and the head is more streamlined [2]. This paper also describes how to calculate aerodynamic drag force using the k-ε turbulence model based on a grid for train head optimization and the connection between the drag force and optimum design. Other than the variation of slenderness ratio, numerous techniques for reducing aerodynamic drag. One of which is the use of bionic circular pits put on the coupling cover [3]. Based on this research, the aerodynamic drag can be lowered by 2%. Aside from that, the length of the high-speed train nose influences aerodynamic performance. The study discovered that lengthening the train nose can substantially minimize aerodynamic drag fluctuations, particularly on the train head [4]. As a result, the length of the train nose substantially impacts the pressure distribution at the train head and the velocity distribution and vortex generation surrounding the train tail. Additionally, the surface pressure distribution and train head flow field are significantly impacted by the difference in windshield configuration and train length [5]. Numerical simulation is a reliable tool for testing design changes during the development stage to achieve the goal of an optimum design. The previous study aids in the analysis of a medium-speed train (MST) in Indonesia by comparing two models prior to validation in a wind tunnel experiment with a scale model size is 1:25 [6]. In a more advanced method, machine learning can be utilized to predict drag in relation to geometric adjustment [7].

This study aims to investigate the aerodynamic phenomena including aerodynamic drag, velocity contour, and pressure contour at the train head of the HST by numerical method. The result of this simulation was compared to the train head of the medium-speed train (MST) by Mario *et al* [6]. In comparison to the MST, the

proposed train head of the HST has a sharper 10^0 angle and a longer nose of 1.5 m.

The structure of this paper is as follows: section 1 describes the background and several recent studies on the aerodynamics of the high-speed train. The general basic theory and the numerical method are then explained in section 2 and section 3, respectively. Finally, in section 4, the numerical results of the aerodynamic train head are explained, followed by the conclusion of this numerical investigation in section 5.

2. BASIC THEORY

A study of the flow characteristics surrounding the high-speed train is required prior to the simulation setup. Generally, the fluid flow has three flow regimes: laminar, transitional, and turbulent. Laminar fluid motion is defined as highly organized fluid motion with smooth layers of fluid. Turbulent fluid motion is defined as high-speed, highly disordered fluid motion characterized by velocity fluctuations. A transitional flow is one that alternates between being laminar and turbulent [8]. The Reynolds number can be used to determine the flow regime.

$$Re = \frac{\rho v L}{\mu} \quad (1)$$

where ρ is the fluid density (kg/m^3); v is the air velocity (m/s); L is the object length (m) and μ is the dynamic viscosity (Pa.s). The Reynolds number of flow fields surrounding the train is greater than 10^6, and the Mach number can be estimated to be less than 0.3 [9]. For small Mach numbers (Ma < 0.3), the flow may be considered incompressible flows [10].

In fluid mechanics, there is an equation called the governing equation. The governing equations include the continuity equation, momentum conservation equation, and energy conservation equation (i.e., Navier-Stokes equation) [8], [11], [12] [13]. Because the flow field in this research is assumed to be an incompressible flow, no energy conservation equation is required. The continuity and the momentum equation determined in equation (1) and (2), respectively.

$$\frac{\partial \rho}{\partial t} + \nabla \cdot (\rho v) = 0 \quad (2)$$

$$\frac{\partial}{\partial t}\int_V \rho v \, dV + \int_S \rho v v \cdot n \, dS = \sum f \quad (3)$$

Because the flow around the train is calculated to be turbulent, a suitable model must be selected. Turbulence models commonly used in the fluid analysis include the k-ε model, the k-ω model, the Large Eddy Simulation (LES), and others [8], [12]. The k-ε turbulence model, on the other hand, is commonly utilized in modelling the flow structure and pressure surrounding a moving train [9]. The simplest complete turbulence model is the standard k-ε turbulence model [14]. This turbulence model is commonly used in the case of computational analysis of the fluid around the train [14], [15], [16]. The flow in this study is in the open air without involving any surrounding infrastructure and the energy equation is neglected, the standard k-ε turbulence model is also used.

The drag force is one of the parameters used in designing a train's aerodynamic effectiveness. Because the train's drag force affects its energy consumption and noise production [17]. The drag force is the force imposed on a body by a flowing fluid in the flow direction [8]. A coefficient is calculated as the judgment criterion. The coefficient of drag Cd is a one-dimensional parameter that depends on drag force, density, velocity, and area [8], [12]. For flows around bodies, the drag coefficient (Cd) is defined as follows [4], [8], [12]:

$$Cd = \frac{D}{\frac{1}{2}\rho v^2 A} \quad (4)$$

where D is the drag force (N); ρ is the fluid density (kg/m^3); v is the air velocity (m/s) and A is the reference area (m^2).

3. NUMERICAL MODEL AND METHOD

In this study, the computational fluid dynamics (CFD) was conducted on ANSYS software. The simulation procedures refer to standard BS EN 14067-4:2013+A1:2018, Railway Applications-Aerodynamics which describes the standard of numerical simulation in the HST case. The numerical simulation was performed according to BS EN 14067-4:2013+A1:2018, using three-dimensional CFD flow simulation and, in general, a validated implementation of a widely accepted turbulence model. The vehicle surface must be modeled with a full-scale maximum deviation of 10 mm from the original shape of the carbody. Aerodynamically significant features on the train side and roof must be modeled; small protruding objects such as antennae, handles, and so on are not required (diameters, gaps, and obstacles smaller than 50 mm). In addition, the geometry of the bogies can be simplified by ignoring features smaller than 100 mm. The domain extensions must extend at least 50 m in each direction from the rolling stock's nose position. The blockage ratio must be less than 0.01.

3.1 High-Speed Train Model

The HST simulation model was arranged in three formations to represent the actual train configuration, as illustrated in Figure-1. The front carriage of the train is the head, with a length of 27.9 m, followed by the middle and the tail carriages, with a length of 25.5 m and 27.9 m, respectively. The cross-section of the carriage has a 3.25 m width and a 4.05 m height.

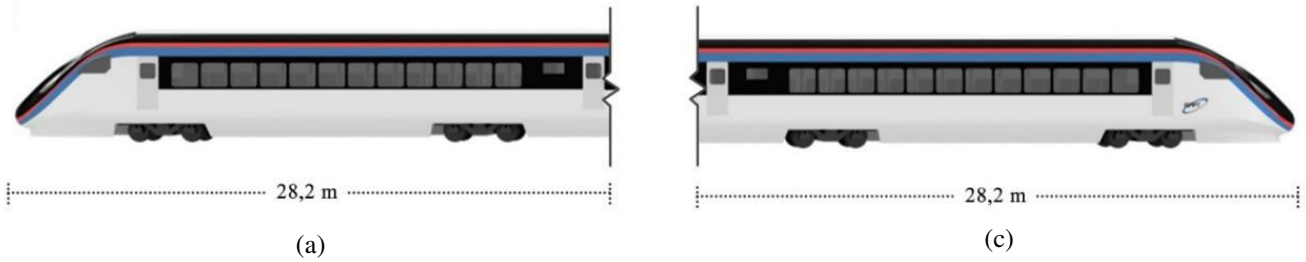

Figure-1. High-speed train geometry (a) front carriage; (b) middle carriage; and (c) tail carriage.

Meanwhile, the cross-section of the train head model is shown in Figure-2. The geometry of the train head is the same as the carriage geometry. In comparison to the medium-speed train which was previously studied by Mario [6], the proposed train head of a high-speed train has a sharper 10^0 angle and a longer nose of 1.5 m. The schematic head train model geometry and the wind tunnel test model of HST and MST are shown in Figure-3.

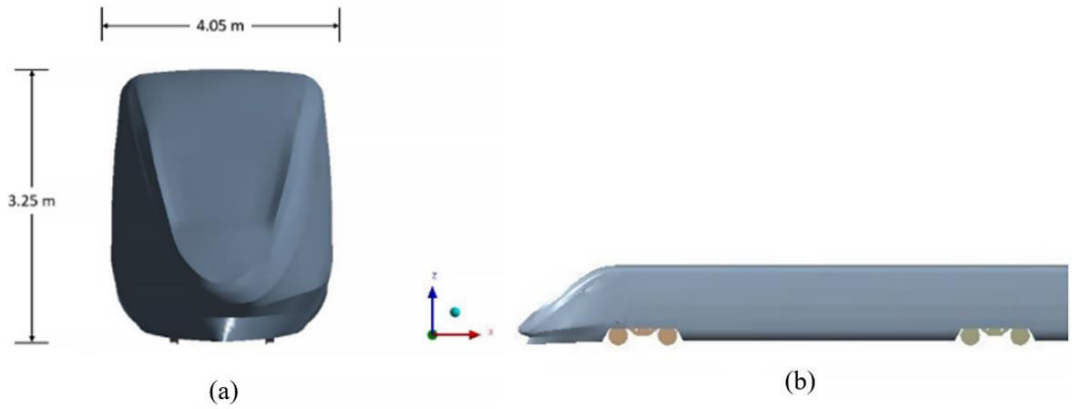

Figure-2. Train head geometry (a) front view and (b) side view.

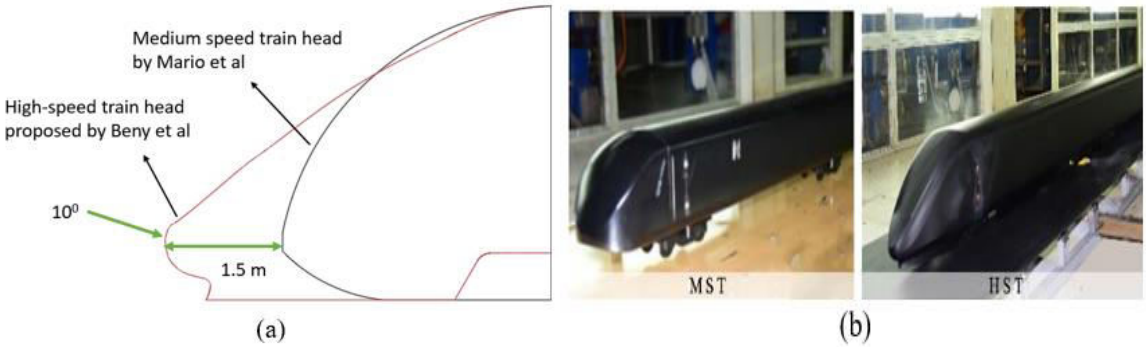

Figure-3. (a) The schematic head train model geometry; and (b) the wind tunnel test model of HST and MST.

3.2 Computational Domain

In this study, the computational fluid dynamics (CFD) was conducted on ANSYS software. The simulation procedures refer to standard BS EN 14067-4:2013+A1:2018, Railway Applications-Aerodynamics which describes the standard of numerical simulation in the HST case. In this simulation, the train model is simplified into Figure-4 by ignoring other parts like the train windows, doors, pantographs, and train connecting, because this study only focuses on aerodynamic phenomena on the train head. Meanwhile, the cowcatcher at the bottom of the train head still exists in order to reduce vortex generation and drag.

The simulation enclosure is created to represent the actual train environment and is used to represent airflow during computational simulations. Therefore, the

domain must be carefully defined to produce an accurate and efficient simulation. The size of the domain must be able to cover all the phenomena needed but not too large because it will take longer computation time. The domain's shape must also correspond to the geometry of the train. The computational domain of the model is presented in Figure-5. The train model is placed at the center of the computational model. According to BS EN 14067-4:2013+A1:2018, the domain boundaries must not physically obstruct the flow surrounding the vehicle. The domain extensions must extend at least 50 meters in each direction from the rolling stock's nose position. The frontal area, also known as the velocity inlet, was positioned 80 meters away from the train's nose. Similarly, the outlet, situated behind the tail end of the model, was placed at a distance of 188 meters. This was to ensure that the wake vortices phenomenon could be captured with adequate space. The enclosure's width was set to 110 meters, and the height was 70 meters.

The numerical simulation result for the blocking ratio must be less than 15%. When the blocking ratio is between 5% and 15%, the results must be improved; if the blocking ratio is less than 5%, correction is unnecessary. The blocking ratio in this study is 0.5%; both the computational domain dimension and the blocking ratio comply with the computational prerequisite. The selection of an appropriate mathematical model is crucial in simulations to ensure the accuracy and validity of simulation results. In computational fluid dynamics simulations to model turbulent fluid flow, turbulence models such as RANS, LES, and DNS are needed as turbulent fluid flow is complex and cannot be accurately predicted by simple Navier-Stokes equations. Turbulence models can improve simulation accuracy by accounting for turbulence effects on fluid flow. The k-ε turbulence model, a type of RANS model, is commonly used in computational fluid dynamics simulations to model turbulent fluid flow by accounting for turbulence viscosity. This model is popular because it is simple and requires shorter computation times than other turbulence models.

To describe the behavior of fluid flow on boundary surfaces, such as solid surfaces, the no-slip solid-wall boundary condition is used as a mathematical model or boundary model. This condition states that the fluid velocity relative to the surface is zero, or there is no flow crossing the surface. The no-slip boundary condition is critical in simulations of fluid flow on solid surfaces as it can affect the distribution of pressure, velocity, and shear stress around the surface. This simulation used a no-slip solid-wall boundary condition with an air inlet velocity of 69 m/s or 250 km/h as required in design speed and a pressure outlet of 101,325 Pa. Uniform inlet velocity and uniform pressure outlet, with the symmetrical wall.

Figure-4. Simplified train model.

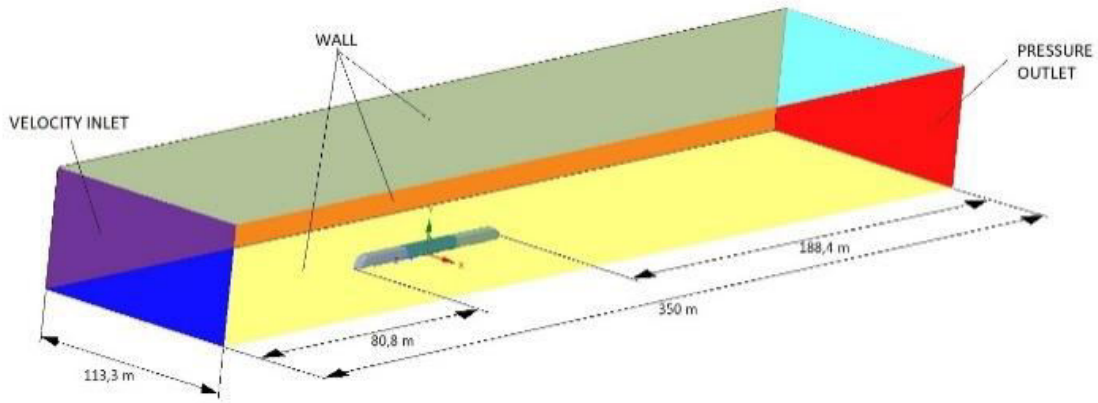

Figure-5. Computational domain.

3.3 Meshing

Mesh generation is an important stage in computational fluid dynamics (CFD) for stable and accurate simulations [18], [19]. One of the steps to validating a model is a mesh independence test. The mesh independence test is a crucial aspect of computational fluid dynamics (CFD) simulations, as it determines the accuracy and reliability of the results [20]. A mesh independence test involves analyzing how the solution changes as the mesh size is increased or decreased. The goal is to determine the minimum number of mesh elements required to achieve an acceptable level of accuracy.

4. RESULT AND DISCUSSIONS

4.1 Mesh Validation

A coarse mesh and a fine mesh must be utilized to evaluate a CFD simulation using a mesh independence test. The coarse mesh will have fewer elements, while the fine mesh will have a higher number of elements. In this case, the results of Cd from the simulation were compared in Table-1.

Table-1. Number of cells and Cd.

Size of cells	Number of cells	Cd
2,750 mm	1.486 million	0.352
2,500 mm	1.549 million	0.347
2,250 mm	1.623 million	0.347
2,000 mm	1.734 million	0.341
1,750 mm	1.904 million	0.343
1,500 mm	2.161 million	0.343

According to the mesh independent test, the value of Cd starts convergence in 1.9 x 10^6 mesh elements, with a mesh size of 1,750 mm. It can be observed from the result above that the value of Cd is converging at 0.343. The graphic plot of the mesh-independent test in ANSYS can be seen in Figure-6. The simulation result converged in 1.904 million cells of mesh, as shown in Figure-7. Further changing the refinement mesh will not significantly affect the result.

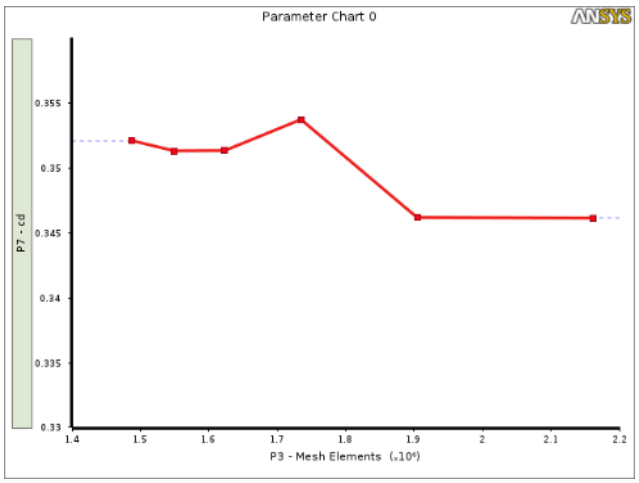

Figure-6. Mesh independence test in ANSYS.

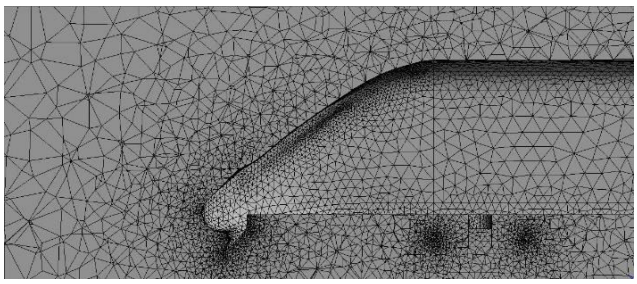

Figure-7. The detail mesh of train model.

4.2 Velocity Result

The velocity profile around the head is complex and affected by several factors, including the shape of the nose, the train's speed, and the properties of the fluid medium in which it travels. Figure-8 depicts the velocity contours of the air around the nose of the HST. In this case, the velocity at the surface of the ground transitioning to blue color indicates zero magnitudes. As the air flows towards the front face of the train the velocity magnitude gradually decreases. A rapid decrease occurs before the air reaches the nose of the train and reaches the stagnation point shown by the thin blue region.

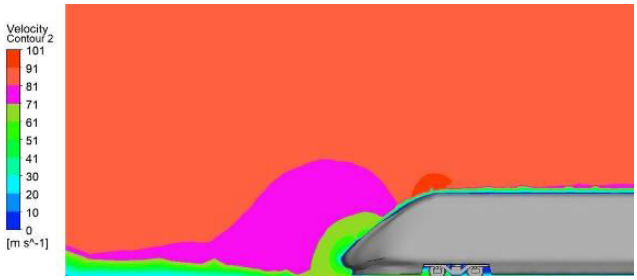

Figure-8. Velocity contour at the train head.

The boundary layer surrounding the nose is thin and goes along the surface body of the HST. The velocity then gradually increases until it reaches the separation point at the top of the train's front nose. As we can see in the image, an area of very high velocity occurs. This is where the air particles escape from the surface friction and rapidly gain acceleration.

4.3 Pressure Result

To design a carbody that can sustain pressure loads caused by the difference in air static pressure between the interior and exterior of the train due to the high train speed, the pressure distribution on the outside of the train must be investigated. Furthermore, to analyze the pressure distribution in this location to avoid window bursts during operation due to excessive pressure. Additionally, this pressure distribution data outside the train can be utilized to design the air conditioning within the train to be comfortable for passengers.

The contour of pressure is shown in Figure-9 which is a red contour at the tip of the nose indicating a sudden increase in pressure. Because of the compression of the air in front of the train, the pressure distribution around the nose of HST is characterized by high pressure

on the frontal area. This is at the point at which the velocity of air rapidly decreases, also known as the stagnation point. The blue zone denotes a sudden pressure drop at the side of the train head and on the carbody's roof. These sudden pressure changes contribute to an increase in drag resistance [21].

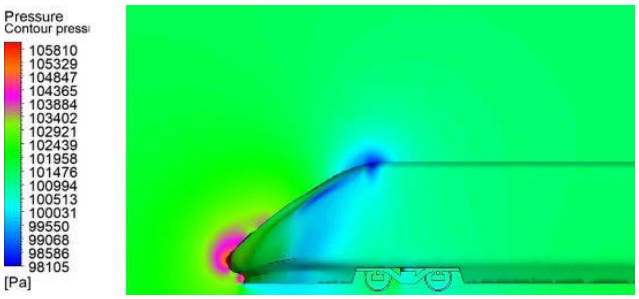

Figure-9. Pressure contour at the train head.

In a perspective view as shown in Figure-10. It can be seen that the highest pressure was at the tip of the nose where the hatch cover of the coupler was placed. A small region of high pressure can be seen at the lower part of the HST windshield. However, the pressure at the windshield is generally the same as the surrounding atmospheric pressure.

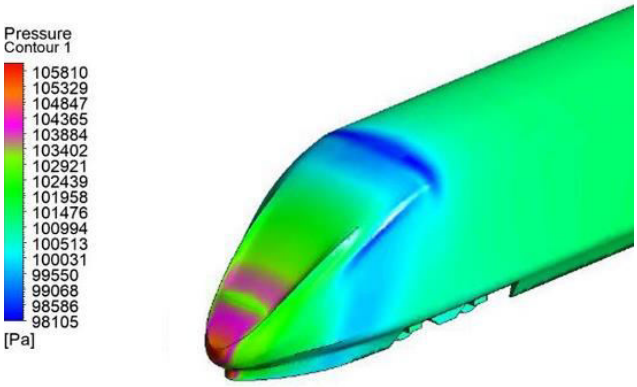

Figure-10. Pressure distribution at windshield area.

Figure-11 depicts the air flows surrounding the train head and carbody. It aids the design engineer in understanding the impact of form modification on airflow. The air will naturally flow under the nose of the train and form huge vortices due to the obstruction of the bogie and wheel structures. To deflect the flow, a cowcatcher shape was placed under the nose to reduce the amount of flow that goes beneath the carriage. Meanwhile, Figure-12 depicts the flow pattern beneath the carriages. The cowcatcher aids in reducing vortex generation and drag. There is, however, a little opening that permits air to travel beneath the carbody. In further development, the visualization will assist the engineer in investigating the airflow, which can assist in the cooling impact of the train brake. The pressure differential between the head and tail ends of the high-speed train influences overall drag performance because it causes a large wake behind the train, which increases drag force.

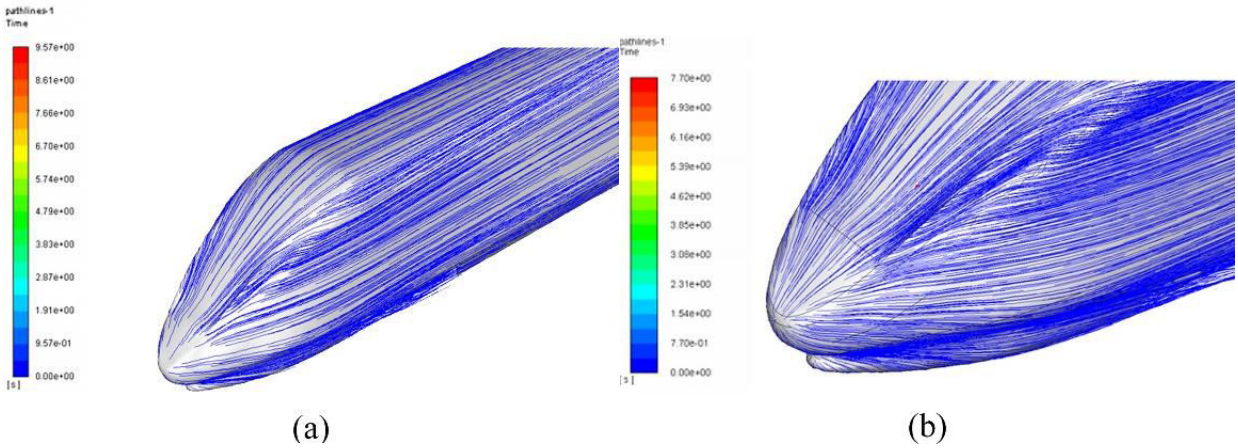

Figure-11. Flow characteristic at the frontal area, (a) streamline from train head to carbody and (b) detailed streamline at the nose and windshield area.

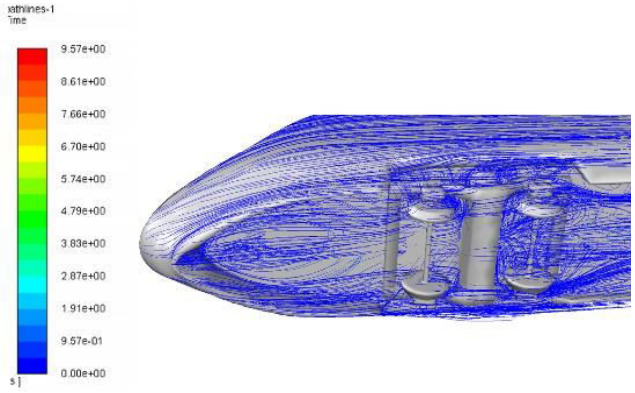

Figure-12. Flow and vortices under the cowcatcher and bogie.

According to Figure-14 flow separation occurs around the lower area of the train's rear head window. At the tail end of the HST, there are vortices generated at the side of the train, which affect the surrounding environment. The turbulence air wake area near the train appears small, so it can reduce pressure drag. The airflow is more rapidly experienced in the laminar flow stage. These contours confirm that drag is reduced when the gap between vortices is also reduced [22].

A wind tunnel experiment employing a scale model size of 1:18 was carried out to validate the numerical method, as illustrated in Figure-13. The coefficient of drag was found to be 0.38 in the experiment, a 10% divergence from the CFD simulation.

Figure-13. HST model experiment setup in the wind tunnel.

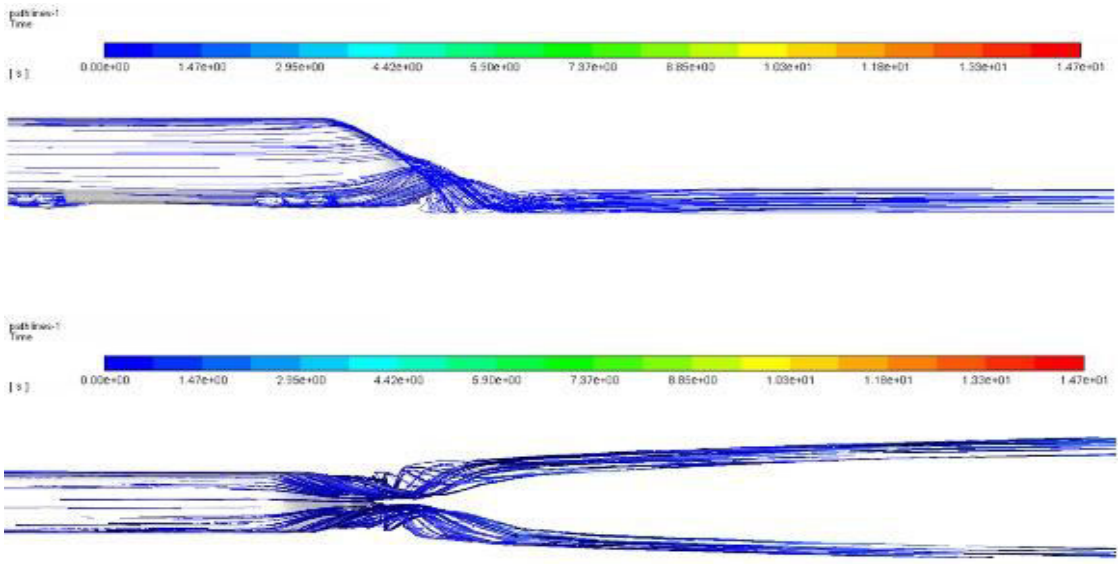

Figure-14. Vortices at the tail-end of the train.

5. CONCLUSIONS

A new high-speed train design has been developed to enhance the aerodynamic performance of the previously designed medium-speed train model. The effectiveness of the design was studied using numerical simulation to investigate the aerodynamic phenomena of a high-speed train head such as aerodynamic drag, airflow patterns, velocity, and pressure profiles.

The simulations highlighted the need for various design tweaks and adjustments to achieve a lower drag coefficient value, minimizing drag and conserving energy. To get the optimum shape, design modifications and optimization were iteratively analysed in CFD simulation. The lower coefficient of drag is achieved by applying a longer nose and a smaller angle of the train nose.

The validity of the simulation was further confirmed by conducting a wind tunnel experiment on a scaled model from the optimum design. The experimental outcome demonstrated a satisfactory level of agreement with the simulation results.

ACKNOWLEDGEMENTS

The research funding, Ansys Fluent software and Wind Tunnel laboratory were provided by the Indonesia National Research and Innovation Agency (BRIN). We thank our colleagues at PT. INKA (Persero) for their insightful discussions during the design's development.

We would also like to thank our research collaborator from Institut Teknologi Sepuluh Nopember (ITS) Surabaya in recognition of their contribution to the carbody model.

REFERENCES

[1] Z. Chen, T. Liu, Z. Jiang, Z. Guo and J. Zhang. 2018. Comparative analysis of the effect of different nose lengths on train aerodynamic performance under crosswind. J Fluids Struct, 78: 69-85, doi: 10.1016/j.jfluidstructs.2017.12.016.

[2] K. Cui, X. Wang, S. Hu and T. Gao. 2012. Aerodynamic performance comparison of head shapes for high-speed train at 500KPH. Advances in Civil, Environmental, and Materials Research (ACEM' 12), no. Baker 2010.

[3] T. Li, D. Qin, J. Zhang and M. Li. 2019. Aerodynamic drag reduction of high-speed train nose with bionic round pits. Comput Sci Eng, 21(3): 31-41, doi: 10.1109/MCSE.2019.2902474.

[4] J. Niu, Y. Wang, L. Zhang and Y. Yuan. 2018. Numerical analysis of aerodynamic characteristics of high-speed train with different train nose lengths. Int J Heat Mass Transf, 127: 188-199, doi: 10.1016/j.ijheatmasstransfer.2018.08.041.

[5] A. Adamu, J. Zhang, F. Gidado and F. Wang. 2023. An investigation of influence of windshield configuration and train length on high-speed train aerodynamic performance. Journal of Applied Fluid Mechanics, 16(2): 337-352, doi: 10.47176/jafm.16.02.1433.

[6] J. Mario, B. Halfina, D. Bahtera, L. Shalahuddin and A. Windharto. 2020. Numerical and experimental analysis of drag force in medium speed train design. in IOP Conference Series: Materials Science and Engineering, IOP Publishing. p. 12031.

[7] S. Adityo, Hendrato, Sucipto and A. Irfan. 2020. Determination of robust weights hidden layers on backpropagation algorithm to analyze coefficient drag high-speed train. in Journal of Physics: Conference Series, Institute of Physics Publishing, Jun. 2020. doi: 10.1088/1742-6596/1511/1/012074.

[8] Y. Cengel, and J. Cimbala. 2013. Fluid mechanics fundamentals and applications. McGraw Hill.

[9] E. Deng, W. Yang, M. Lei, Z. Zhu and P. Zhang. 2019. Aerodynamic loads and traffic safety of high-speed trains when passing through two windproof facilities under crosswind: A comparative study. Eng Struct, 188: 320-339, doi: 10.1016/j.engstruct.2019.01.080.

[10] J. H. Ferziger, M. Perić and R. L. Street. Computational Methods for Fluid Dynamics.

[11] E. Deng, W. Yang, M. Lei, Z. Zhu and P. Zhang. 2019. Aerodynamic loads and traffic safety of high-speed trains when passing through two windproof facilities under crosswind: A comparative study. Eng Struct, 188: 320-339, doi: 10.1016/j.engstruct.2019.01.080.

[12] J. H. Ferziger, M. Perić and R. L. Street. 2019. Computational methods for fluid dynamics. Springer.

[13] M. Tauviqirrahman and K. Ma. 2022. Numerical simulation of effect of artificial reef arrangements on wake region characteristic around the combined tube reef with zig-zag formation. 17(16), [Online]. Available: www.arpnjournals.com

[14] J. K. Choi and K. H. Kim. 2014. Effects of nose shape and tunnel cross-sectional area on aerodynamic drag of train traveling in tunnels. Tunnelling and Underground Space Technology, 41(1): 62-73, doi: 10.1016/j.tust.2013.11.012.

[15] J. Muñoz-Paniagua, J. García and A. Crespo. 2014. Genetically aerodynamic optimization of the nose shape of a high-speed train entering a tunnel. Journal of Wind Engineering and Industrial Aerodynamics, 130: 48-61, doi: 10.1016/j.jweia.2014.03.005.

[16] F. Liu, S. Yao, J. Zhang and Y. ben Zhang. 2016. Effect of increased linings on micro-pressure waves in a high-speed railway tunnel. Tunnelling and Underground Space Technology, 52: 62-70, doi: 10.1016/j.tust.2015.11.020.

[17] J. Niu, Y. Wang, L. Zhang and Y. Yuan. 2018. Numerical analysis of aerodynamic characteristics of high-speed train with different train nose lengths. Int J Heat Mass Transf, 127: 188-199, doi: 10.1016/j.ijheatmasstransfer.2018.08.041.

[18] C. Lorsung and A. Barati Farimani. 2023. Mesh deep Q network: A deep reinforcement learning framework for improving meshes in computational fluid dynamics. AIP Adv, 13(1), doi: 10.1063/5.0138039.

[19] O. M. Oyewola, P. M. Singh, O. S. Ismail, and K. Abu. 2021. Numerical simulation of forced convective flows over a pair of side-by-side heated circular cylinders. 16(13), [Online]. Available: www.arpnjournals.com

[20] A. Seeni, P. Rajendran and H. Mamat. 2019. CFD Letters A CFD Mesh independent solution technique for low reynolds number propeller. CFD Letters. 11: 15-30.

[21] M. Kwak, S. Yun, and C. Park. 2015. Optimal design for the nose shape of commercial high-speed train using function of train configuration. Journal of the Korean society for railway, 18(4): 279-288, doi: 10.7782/jksr.2015.18.4.279.

[22] J. Muñoz-Paniagua and J. García. 2020. Aerodynamic drag optimization of a high-speed train. Journal of Wind Engineering and Industrial Aerodynamics, vol. 204, doi: 10.1016/j.jweia.2020.104215.